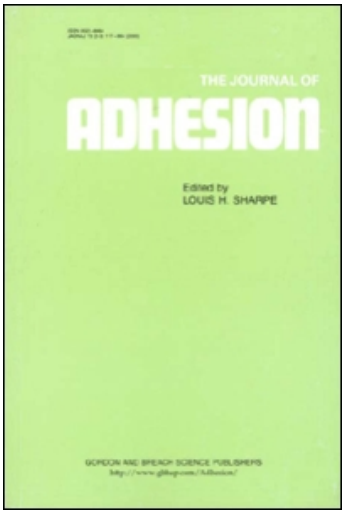

The Journal of Adhesion
Publication details, including instructions for authors and subscription information:
http://www.informaworld.com/smpp/title~content=t713453635

An Adhesion Process for Space Solar Cells

H. Zhao[a]; Z. Fu[a]; P. B. Li[a]; Y. Z. Zhao[a]
[a] The Robotics Institute, School of Mechanical Engineering, Shanghai Jiao Tong University, Shanghai, P. R. China

To cite this Article Zhao, H. , Fu, Z. , Li, P. B. and Zhao, Y. Z.(2007) 'An Adhesion Process for Space Solar Cells', The Journal of Adhesion, 83: 12, 1003 — 1029
To link to this Article: DOI: 10.1080/00218460701749479
URL: http://dx.doi.org/10.1080/00218460701749479

The Journal of Adhesion, 83:1003–1029, 2007

ISSN: 0021-8464 print/1545-5823 online
DOI: 10.1080/00218460701749479

Taylor & Francis
Taylor & Francis Group

An Adhesion Process for Space Solar Cells

H. Zhao
Z. Fu
P. B. Li
Y. Z. Zhao
The Robotics Institute, School of Mechanical Engineering, Shanghai Jiao Tong University, Shanghai, P. R. China

A type of silicone adhesive was used for bonding anti-irradiation cover glasses to space solar cells. A new adhesion process for solar cells was designed, and implemented by means of an automated coating and bonding system based on an industrial robot. On the basis of non-Newtonian fluid theory, flow models of three subprocesses were created, and the commercial finite element analysis code Adina was employed to simulate the whole process. The purpose of the investigation was to acknowledge the mechanism of the adhesion process and identify correlative factors that influence the adhesion quality, to provide a basis for optimization of the adhesion process. A simulation platform was created, to make it possible to evaluate or predict the adhesion quality of space solar cells when the dimensions of the solar cells and the adhesive were changed.

Keywords: Adhesion; Dynamic mechanical analysis; Non-Newtonian fluid; Silicones; Space solar cells

1. INTRODUCTION

The power supply system is a very important sub-system in space probes and solar cells are widely used as space power [1–4]. In the outer space (150 kilometers far away), however, the irradiation intensity of the sun is about 1360 W/m^2, 13–17 times as great as that on the earth [5–6]. In the extreme environment of space, temperature varies greatly and there are many high-energy particles, which require that

Recevied 9 May 2007; in final form 28 September 2007.

Address correspondence to Yanzheng Zhao, The Mechanical Building #906, The Robotics Institute, Shanghai Jiao Tong University, #800 Dongchuan Road, Shanghai 200240, P. R. China. E-mail: yzh-zhao@sjtu.edu.cn

the solar cell must have consistent quality and anti-irradiation characteristics. To protect solar cells from harmful effects in the space environment, ultra-thin and radiation-stable cover glasses are bonded to solar cells to shield the cell from ionizing radiation and intense ultra-violet light.

The traditional method of bonding an anti-irradiation cover glass to a silicon solar cell is by means of a silicone adhesive or Teflon® [7–9]. Advanced bonding techniques, such as electrostatic bonding, may be employed to bond the cover glass directly to a silicon or gallium arsenide solar cell if the cover glass and solar cell have matching thermal expansion coefficients [10–13]. In the work described in this article, a cover glass was bonded to a silicon solar cell with a silicone adhesive. The process for bonding a solar cell to be used in space is as follows: coat the active surface of the solar cell with adhesive; bond an anti-irradiation cover glass to the solar cell; heat to solidify; and check and measure. The requirements for a solar cell assembly are as follows:

i. The adhesive layer should be even, and its thickness should never exceed 150 μm.
ii. The edge-alignment error between the solar cell and the cover glass should be no more than 300 μm.
iii. Bubbles in the adhesive layer must be strictly controlled, so that the number of bubbles of 1 mm diameter is no more than two and the number of bubbles of 0.5 mm diameter is no more than three.
iv. The breakage rate of cover glasses should be no greater than 1%, and the breakage rate of solar cells no greater than 0.5%.
v. The adhesive must not flow out and stain the cover glass or solar cell.

We would like to make it clear that this work is concerned only with the processes for assembly of the solar cells and not with the debonding of the components of the cells.

Many technologies for adhesive coating and bonding have been developed to be used in various industrial applications. The silk screen printing technique is by far the most widely used for coating with adhesives, but it is difficult to control the uniformity of the thickness of the adhesive layer in practical operation [14]. Spray-coating technology is also extensively employed to deposit adhesive materials on substrates owing to its advantages of coating uniformity, good stability, and so on. The spin-coating technique is used to deposit adhesives on substrates by making use of the centripetal force generated by rotating the substrate platform [15]. These techniques are very

suitable for depositing adhesives on round or planar parts, but it is hard to form a clearly defined, straight border line in the marginal area. Many experiments have proved that spray- and spin-coating techniques are not suitable for adhesive coating of space solar cells. Coating with a syringe is another popular technique, which is widely used in medical, chemical, industrial applications, and so on [16–18]. Syringe-coating can precisely control the volume of deposited adhesive and the coated area and can make an ideal adhesive layer that meets the requirements for thickness and uniformity that is suitable for bonding space solar cells. Bonding of solar cells under vacuum is not recommended because of the complexity and high cost of producing a vacuum and of the sealed equipment required.

In the work described in this article, we adopted the method of coating using a syringe; we used a back-and-forth pattern for applying the adhesive coating, and performed the bonding operation under non-vacuum conditions with the cover glass held at an incline to avoid creation of air bubbles. An automated coating and bonding system (ACBS) was developed to perform the above operations for producing bonded solar cells [19–21]. Experiments have shown that an ACBS can meet the bonding requirements of space solar cells.

In general, the meaning of adhesion quality of space solar cells includes three aspects: (1) the thickness and uniformity of the adhesive layer, air bubbles in the adhesive layer, and the edge-alignment of the cover glass with the solar cell; (2) the adhesion strength and residual stress between the cover glass and the solar cell [22–24]; and (3) the adhesion ability to resist the thermal stress cycle in an outer space environment [25–27]. The first point is the only adhesion quality of relevance to the automated coating and bonding system.

Many papers address fluid flow in various adhesive-coating and bonding applications. Some publications have discussed the constitutive relationship of the fluid in the coating process and have used a power-law model or a viscoelastic model [28–29]. Some researchers have modelled the coating process in order to describe or predict the characteristics and quality of the coating [30–32]. In addition to experimental investigations, numerical simulations have been performed, mostly based on computational fluid dynamics (CFD), to analyse the coating process and to discover the operating parameters influencing the coating quality. Some of these simulations have used the commercial CFD code FLUENT [33–34], and some have used finite element analysis (FEA) [35]. In some coating applications, such as trihelical coating, gravure roll coating, and spin coating, the most relevant results of the experiments are the thickness, uniformity, and quality of the coated film, and the important parameters affecting

them [36–38]. As for the bonding process, various bonding techniques are used in the manufacturing processes of solar cells and other thin films. However, few investigations have been conducted into the bonding of a solar cell and a cover glass with silicone adhesive. Considering the particular features of the bonding technique, the non-Newtonian characteristics of the fluid, and the microscopic behaviour of the surface tension of the adhesive, it is necessary to analyse the flow of the adhesive, so as to take account of the influence of fluid flow on the final adhesion quality.

The whole adhesion process consists of two sub-processes: coating of the adhesive, and bonding of the solar cell. The former process itself consists of two sub-processes: pipe flow and planar spreading. On the basis of non-Newtonian fluid theory, we have created flow models of the three sub-processes, and the commercial FEA code Adina (Adina china, Beijing, China) was employed to simulate the whole process. The simulation results were validated *via* theoretical and experimental data. The objective of the analysis of the process was to acknowledge the mechanism of the adhesion process and find the correlative factors that influence the adhesion quality, and to allow us to create a simulation platform to make an evaluation or prediction of the adhesion quality of space solar cells when the dimensions of the solar cells and the adhesive are changed. Furthermore, the results of the analysis in this article could be used to optimize the parameters of the adhesion process.

2. MATERIAL PROPERTIES

2.1. Space Solar Cells

In the past, solar cells were made traditionally from silicon and had a low photovoltaic conversion efficiency of about 10% [39]. In the last 20 years, various new types of solar cells that make use of new materials or structures have arisen, such as GaAs/GaAs, GaAs/Ge, InP/InP, InP/Si, CdS/CdTe, $CuInSe_2$, spotlight and amorphous-silicon-film solar cells, which have a high photovoltaic conversion efficiency (GaAs cells can have an efficiency of up to 30% [40]) and other excellent performance features [41–43]. So far in China, however, most of the solar cells used in outer space have been made of crystalline silicon (Fig. 1), which has a photovoltaic conversion efficiency of 12–15% [44–46]. Besides, owing to the high launch cost, the mass of solar cells must be reduced, which has resulted in a trend in which space solar cells have become thinner and thinner, from 200 μm to 120–150 μm thick in the third generation [46]. The continuous development of GaAs

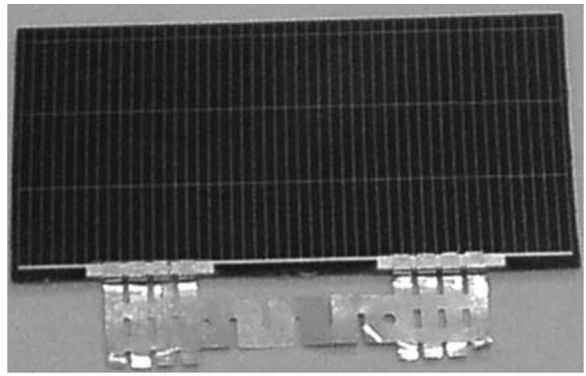

FIGURE 1 A space solar cell.

solar cells has led to ultrathin films 6–8 μm thick or even less [47–48]. How to obtain a high conversion efficiency and ratio of power to mass while reducing the thickness to reduce the mass of the cells is still a focus of research [49–50]. In our task, silicon solar cells (Shanghai Institute of Space Power, Shanghai, China) of four different dimensions were bonded; these four dimensions are designated A, B, C, and D, and described in Table 1.

2.2. Anti-Irradiation Cover Glass

The standard properties of anti-irradiation cover glasses should include excellent optical transmission, radiation stability, low solar absorbance, and high emissivity [10]. An important feature of cover glasses is their thermal expansion coefficient. The newly designed CMZ and CMG cover glasses (QIOPTIQ Space Technology, Bodelwyddan, UK) have a thermal expansion coefficient matching that of silicon and gallium arsenide, respectively, which allows the cover glass to be directly

TABLE 1 Dimensions of Space Solar Cells Used

Type	Length (mm)	Width (mm)	Thickness (mm)
A	40	20	0.20
B	50	25	0.20
C	50	23	0.20
D	40.8	20.6	0.18

bonded to a solar cell *via* advanced bonding techniques such as electrostatic bonding [8–10]. These two cover glasses were Pilkington Borosilicate Glass types (Pilkington, Merseyslos, UK) which have high emissivity, ultra violet, electron and proton radiation protection, cerium dioxide stabilization to prevent colour centre formation, and enhanced strength for increased yield at bonding. There has been a trend for cover glasses to become thinner, from 120 μm to a range of 50–70 μm [46].

2.3. Silicone Adhesive

A proprietary adhesive was employed to bond the cover glass to the solar cell; the adhesive material used was a silicone rubber (GPJ040, Shanghai Institute of Space Power Shanghai, China). Some researchers have studied the evolution of the performance of silicone rubber in a space environment [51]. The most important concern for operation of the adhesive is its rheology, *i.e.*, how its viscosity varies with time, shear rate, and temperature [52]. In order to satisfy the requirements of automated manufacturing, the viscosity was changed from 7500 cP to 3000 cP. The temperature needed to be kept at about 24°C. The adhesive needed to be applied in a timely fashion, because its viscosity increased significantly after 3–4 hours. After bonding of the cover glass to the solar cell, the bonded assembly was moved into a heated box so the adhesive could solidify. The transmissivity of the solidified adhesive was greater than 92% under irradiation with ultraviolet radiation [51].

An experimental device called advanced rheology expansion system (ARES TA Instruments, New Castle, Delaware, USA) was employed to test the rheological characteristics of the silicone adhesive. ARES is an extremely capable and versatile all-purpose rheometer appropriate for characterizing a diverse variety of materials over a broad spectrum of medium to high viscosity fluids, including polymer melts, composites, solids, and reactive materials. Any of the available temperature control options can be used with the ARES rheometer. It can measure samples' static shear viscosity, normal force, shear modulus, complex viscosity, energy storage modulus, loss modulus, damp, etc. Moreover, the system can accurately supply a broad range of frequency and achieve smaller dynamic strain than that of a stress rheometer (temperature: $-150 \sim 600$°C; torque: $0.2 \sim 2000\,\mathrm{g \cdot cm}$; normal force: $2.0 \sim 2000$ g). Experiments included three sweeping types: strain rate sweeping, strain sweeping, and time sweeping. Making strain rate sweeping on the adhesive, we obtained the experimental data of the apparent viscosity with shear rate, and fitted the relational curve of

the apparent viscosity, η, and shear rate, γ (Fig. 2a). Making strain sweeping on the adhesive, we obtained the experimental data of the shear modulus, G, with strain, ε (see Fig. 2b). Keeping the strain at 10%, made time sweeping on the adhesive, and we obtained the data of the shear modulus, G, with time, t (see Fig. 2c). It was clearly seen that the shear modulus, $G(G = G' + i \cdot G'', G = |G|)$, remained stable during a change of strain from 5 to 60% for a short time of minutes.

If the silicone adhesive is regarded as a power-law fluid, two constitutive parameters could be obtained by curve fitting in Fig. 2a: the consistency $\mu = 3.1622\ \text{Pa} \cdot \text{s}^n$ and the power-law index $n = 0.9893$. If a viscoelastic model is adopted, the adhesive has two constitutive parameters: the shear modulus, G, and the bulk modulus, K. By analysing experimental data in Fig. 2b and c, we obtained $G = 19.8397\ \text{Pa}$. If the adhesive is incompressible, then K goes to infinity. The surface tension, σ_{st}, of the adhesive was also measured by a tensiometer based

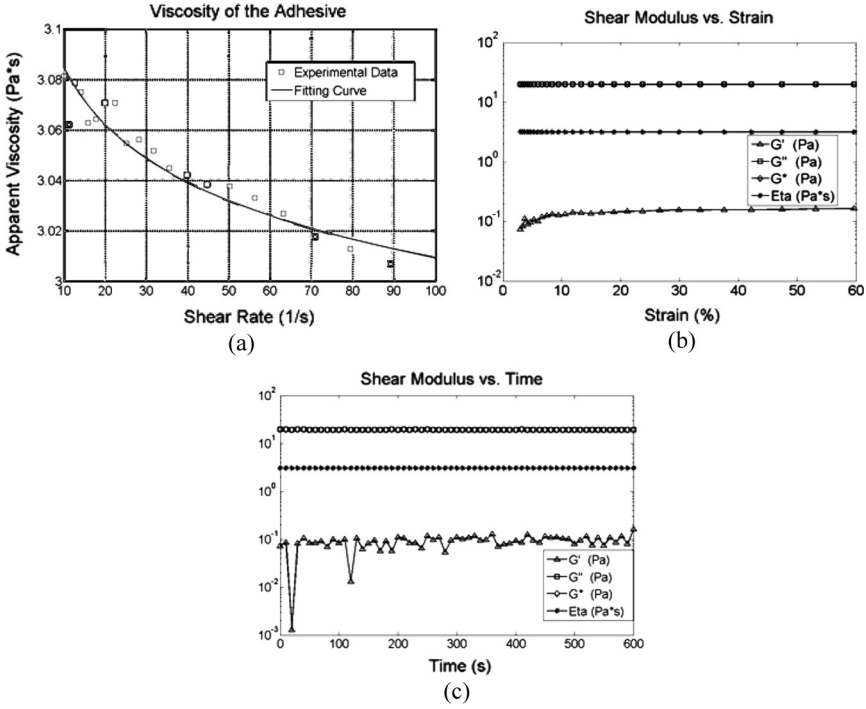

FIGURE 2 Rheological properties of silicone adhesive: (a) apparent viscosity vs. shear rate, (b) shear modulus vs. strain, and (c) shear modulus vs. time. Eta means apparent viscosity.

on the ring method (Sigma 703a, KSV Instruments, Helsinki, Finland). The value of surface tension kept decreasing until it reached 0.016 N/m in a stable state at room temperature.

3. DESIGN AND IMPLEMENTATION OF THE ADHESION PROCESS

3.1. A New Adhesion Process

The traditional way to bond anti-irradiation cover glasses to space solar cells is manual work, which has many disadvantages. The adhesive layer's thickness and uniformity cannot be precisely controlled, the edge-alignment error is large, and it is easy to bring bubbles into the adhesive layer by manual operation. Besides, the solar cell is easily stained by outflow of adhesive and easily broken by hands because of its brittleness. Therefore, it is necessary to perform production with modern automated manufacturing equipment, and to develop a new adhesion process suitable for automated manufacturing.

After many tryouts, we found a coating technique and bonding method that were suitable for space solar cells. The adhesive was deposited onto the solar cell by means of a syringe under a pressure difference. The pattern of application of the adhesive deposited on the solar cell was designed to be a back-and-forth pattern, which was fitted to the rectangular shape of the solar cell. The area of the coating was adjusted by changing the number of lines of adhesive, n_c, the spacing between lines, D, and the distance from the edge, δ (Fig. 3.) Three parameters could be adjusted according to different dimensions of solar cells and adhesive.

The bonding operation was performed under non-vacuum conditions to avoid the complexity and cost of a vacuum system. We have devised a new method of bonding (Fig. 4), where the cover glass is kept close to the adhesive layer at an inclination angle, α. When the cover glass partially contacts the adhesive layer, it is released to allow it to fall onto the adhesive layer freely under gravity. This technique effectively suppresses the formation of air bubbles in the adhesive layer.

3.2. Automated Coating and Bonding System (ACBS)

An ACBS was developed to realize the above adhesion process (see Fig. 5). This system consisted of five parts: an XYZ three-axis industrial robot platform, coating and bonding devices, a control system, a pneumatic system, and industrial-personal-computer (IPC) software.

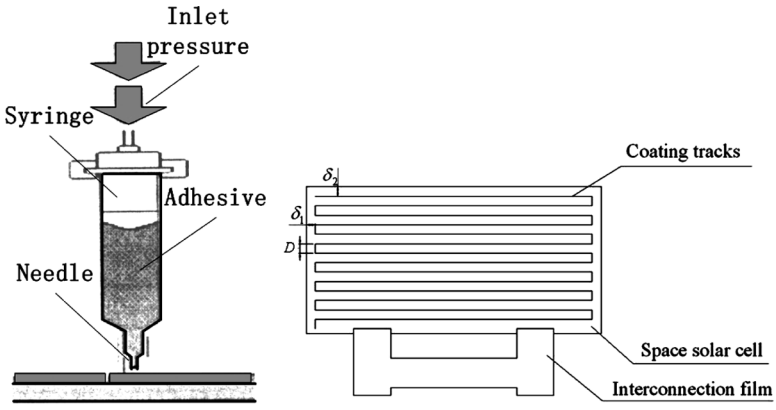

FIGURE 3 Method of syringe-coating: (a) Coating with a syringe, and (b) Pattern of deposited adhesive.

The system adopted a three-axis Cartesian coordinate industrial robot (DASATECH Co., Ltd., Seoul, S. Korea). The robot was a motion control system, dealing with the syringe needle's moving trajectory and speed control, and position control and speed control of the vacuum suction cup. Coating devices mainly consisted of a positioning mechanism fixed on the Z-axis of the robot, some actuating components (namely syringe), and some pneumatic components such as the electromagnetic valve, pressure valve, etc. They were used to coat the cells with silicone adhesive. In order to improve the coating efficiency, six syringes were installed on the positioning mechanism in an array. These syringes were AirFree^{TM} syringe reservoirs of 10 cc in volume (Fishman Corporation, Hopkinton, MA, USA). The inner diameter of the syringe needles was determined by the viscosity of the adhesive. To make the adhesive flow out of the syringe needles

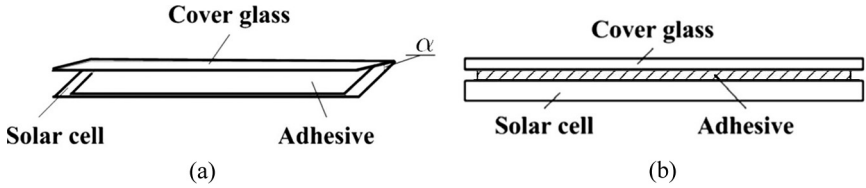

FIGURE 4 Inclined covering technique: (a) Covering at an inclination angle, and (b) Cover glass falling freely under gravity.

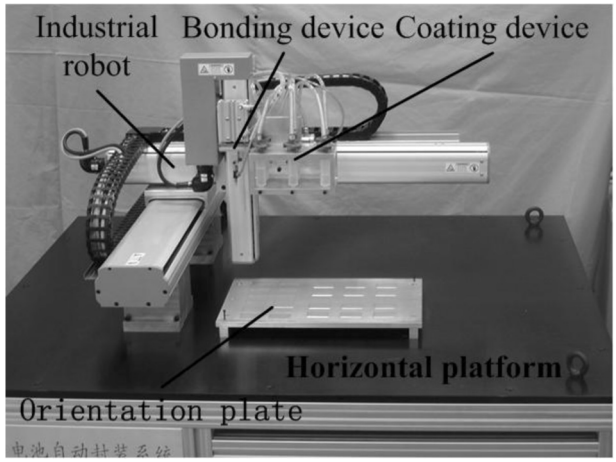

FIGURE 5 A photograph of the ACBS.

in a desired speed range under a prescribed pressure at the upper inlet of the syringe, we tried needles of different inner diameters ranging from 0.05 mm to 0.8 mm, and finally chose the 0.25-mm one. A set of suitable parameters obtained from the experiments are given in Table 2. Bonding devices mainly consisted of an actuating mechanism fixed on the Z-axis, some pneumatic components such as the vacuum suction cup, electromagnetic valve, pressure valve, etc. They were responsible for bonding the working surface of the space solar cells with anti-irradiating cover glasses. Experimentally it was found that an inclination angle of about 10 degrees was suitable for the bonding operation, but the angle needed fine adjustments in accordance with different adhesive, operating conditions, and solar cells of different dimensions. A large steel plate was used as the base of the robot system. The plate must be horizontal as it might influence the bonding

TABLE 2 Coating Operating Parameters

Parameters	Value
Viscosity of adhesive (μ)	3Pa·s
Inner diameter of the needle (Rn)	0.25 mm
Inlet applied pressure (p_L)	0.4 MPa
Needle moving speed (Vn)	2.8 mm/s
Interval between neighbor adhesive lines (D)	0.9 mm
Boundary margin (δ_1, δ_2)	(1.40 mm, 1.45 mm)

quality of the space solar cells. The pneumatic system had three tasks: supplying uniform air pressure for the coating subsystem, driving the air cylinder when bonding, and providing negative pressure for the vacuum suction cup. The pressure switches of the pneumatic system must be closely coordinated with the actions of the robotic system to accomplish the whole process. This coordination was controlled by predefined software on the IPC.

3.3. Performance Evaluation

Many experiments were carried out to test the ACBS and our approach to the adhesion process. A bonded solar cell of one particular size is shown in Fig. 6. We performed experimental tests of the following aspects: the thickness of the adhesive layer, bubbles in the adhesive layer, the edge-alignment error between the solar cell and the cover glass, the breakage rates of solar cells and cover glasses, outflow of adhesive, and the efficiency and reliability of the ACBS. The thickness of the adhesive layer and the edge-alignment error between the solar cell and the cover glass were measured by a precise vernier caliper with a resolution of 1 μm under a microscope. The edge-alignment error generated by the ACBS was an average value of 100 films in the length/width direction. The air bubbles were also observed under a microscope to judge the sizes and number of the bubbles. The breakage rate including solar cells and cover glasses was counted per 200 films. Any cracks existing in solar cells and cover glasses were inspected under a microscope. The outflow of adhesive was observed by the eye. The efficiency of production was measured by how many

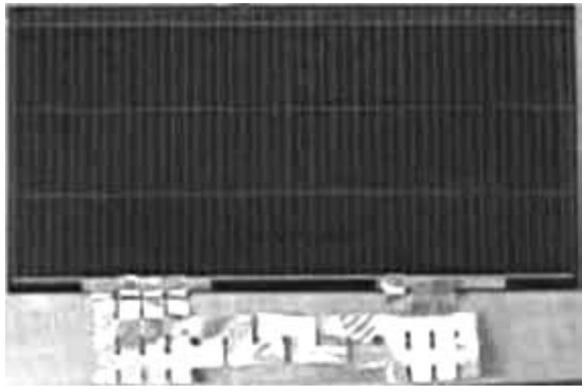

FIGURE 6 A bonded solar cell (50 mm × 25 mm).

TABLE 3 Experimental Results Obtained with the ACBS

Item measured	Results for the ACBS	Results for manual method
Thickness of adhesive layer	100–130 μm	100–150 μm
Bubbles	None (diameter 0.5–1 mm)[a]	Few
Edge-alignment error	Average in length direction: 13 μm Average in width direction: 19 μm	100–500 μm
Breakage rate (solar cells and cover glasses)	0%	4%
Outflow	None[b]	Often (need to clean adhesive)
Efficiency	480 films per day	200 films per day
Reliability	Excellent	Bad

[a]There were no air bubbles of diameter 0.5–1 mm or larger.
[b]There should be no outflow if the worker's procedure is correct.

qualified films were manufactured continuously per day in the normal working procedure. The reliability indicated whether the quality of manufactured films was consistent. Table 3 shows the experimental results. Some corresponding features of traditional manual bonding are also given for comparison. It can be clearly seen that the performance of the ACBS is better than that of the traditional manual bonding.

4. PROCESS ANALYSIS

To make clear the detailed progress of the adhesion process, we intended to model the whole process of bonding solar cells and acknowledge all the parameters that affected the adhesion quality, so as to do a parametric study on the adhesion process to optimize relevant parameters or evaluate/predict the adhesion quality *via* simulation.

4.1. Pipe Flow

4.1.1. Theoretical Modelling and Solution

The flow of the adhesive in the syringe can be divided into three sections: the top wide section, the middle transition section, and the bottom needle section (Fig. 7). It is assumed that the flow in all three sections is axially symmetric and that the pipe flow here is laminar. We adopt a cylindrical coordinate system (r, θ, z) to describe the pipe flow.

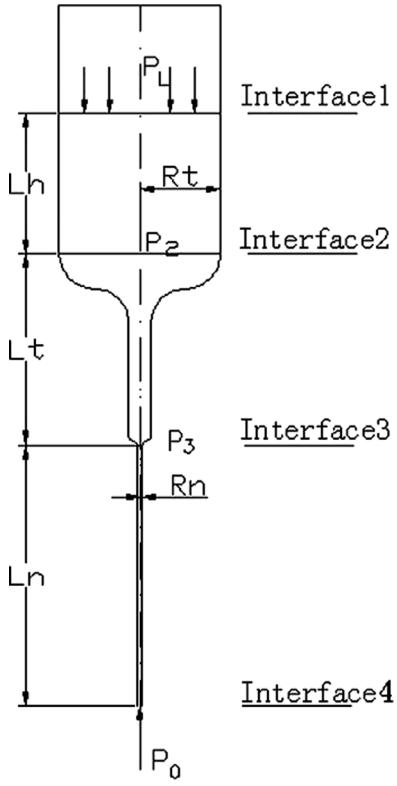

FIGURE 7 Diagram of the pipe flow in the syringe.

Consider the top wide section of the syringe in Fig. 7. It is obvious that the diameter of the wide section is far greater than that of the needle below, so the inlet surface of fluid falls very slowly, and the fluid flow could be regarded to be static in each short time. Therefore, the pressure of the Interface 2 shown in Fig. 7 could be $P_L + \rho g L_h$. Besides, P_L is far greater than $\rho g L_h$, so the latter could be ignored, that is, $P_2 \approx P_{\mathrm{L}}$.

In the middle transition section, the flow speed of the adhesive increases from the wide area to the narrow entrance. Meanwhile, the pressure of fluid diminishes, so the pressure in the Interface 3 is less than in the Interface 2, that is, $P_3 < P_2 (L_t = 47\,\mathrm{mm})$.

Finally, consider the fluid flow in the needle ($L_n = 21\,\mathrm{mm}$). According to our assumption, the flow of fluid is steady, thus the flow speed along the r-direction is regarded to be zero, and we only need to consider the flow of adhesive along the z-direction. Assuming the adhesive

is incompressible, then its density is a constant; gravitation can also be ignored considering the high pressure difference between inlet and outlet; the flow does not change with time while keeping the applied pressure unchanged, which can be regarded as steady flow.

Thus, the velocity field in the needle can be simplified to [52]

$$u_z = u_z(r), \quad u_r = u_\theta = 0.$$

According to the equation of momentum transfer in the z-direction,

$$\rho\left(\frac{\partial u_z}{\partial t} + u_r\frac{\partial u_z}{\partial r} + u_z\frac{\partial u_z}{\partial z}\right) = -\frac{\partial p}{\partial z} + \frac{1}{r}\frac{\partial}{\partial r}(r\tau_{rz}) + \frac{\partial \tau_{zz}}{\partial z} + F_z, \tag{1}$$

we have

$$\frac{\partial p}{\partial z} = \frac{1}{r}\frac{\partial}{\partial r}(r\tau_{rz}). \tag{2}$$

Because p is a function of z only, by integration, Eq. (2) becomes

$$\tau_{rz} = \frac{r}{2}\frac{dp}{dz} + C. \tag{3}$$

Taking the Power Law model to represent the constitutive relationship of the adhesive, we have [53]

$$\tau_{rz} = \mu \cdot \dot{\gamma}_{zr}^{n} = \mu \cdot \left|\frac{\partial u_z}{\partial r}\right|^{n-1}\frac{\partial u_z}{\partial r}, \tag{4}$$

where μ is the consistency, and n is the power law index.

Combining Eq. (3) and Eq. (4), and integrating we obtain

$$u_z = \frac{n}{n+1}\cdot\left(\frac{1}{2\mu}\frac{dp}{dz}\right)^{\frac{1}{n}}\cdot\left(-r^{\frac{n+1}{n}}\right) + C', \tag{5}$$

where C' is a constant of integration.

The boundary condition of the flow in the needle is

$$u_z|_{r=R_n} = 0. \tag{6}$$

Putting Eq. (5) into Eq. (6), the constant C' can be worked out, thus Eq. (5) becomes

$$u_z = \frac{n}{n+1}\left(\frac{1}{2\mu}\frac{dp}{dz}\right)^{\frac{1}{n}}\left(R_n^{\frac{n+1}{n}} - r^{\frac{n+1}{n}}\right) \tag{7}$$

which is the velocity field of the flow in the needle.

According to the formula of flow rate

$$Q = \int_S \int u_z dS = \int_0^{R_n} u_z \cdot 2\pi r \cdot dr. \tag{8}$$

Putting Eq. (7) into Eq. (8), by integration, we have

$$Q = \pi \left(\frac{1}{2\mu} \frac{dp}{dz} \right)^{\frac{1}{n}} \frac{n}{1+3n} R_n^{\frac{1+3n}{n}}. \tag{9}$$

We know that $\frac{dp}{dz} \approx \frac{\Delta p}{L_n} = \frac{P_3 - P_0}{L_n}$. However, P_3 is unknown. We may put the transition section and the needle together, thus the pressure gradient can be written as

$$\frac{dp}{dz} \approx \frac{P_3 - P_0}{L_n} \approx \frac{P_2 - P_0}{L_n + L_t} \approx \frac{P_L - P_0}{L_n + L_t},$$

where P_L is the inlet pressure, P_0 is the atmospheric pressure, L_n is the length of the needle section, and L_t is the length of the transition section.

Therefore, Eq. (7) and Eq. (9) can be written as

$$u_z = \frac{n}{n+1} \left(\frac{1}{2\mu} \cdot \frac{P_L - P_0}{L_n + L_t} \right)^{\frac{1}{n}} (R_n^{\frac{n+1}{n}} - r^{\frac{n+1}{n}}) \quad \text{and} \tag{10}$$

$$Q = \pi \left(\frac{1}{2\mu} \cdot \frac{P_L - P_0}{L_n + L_t} \right)^{\frac{1}{n}} \frac{n}{1+3n} R_n^{\frac{1+3n}{n}}. \tag{11}$$

It is easily found that the velocity, u_z, and flow rate, Q, are relevant to the parameters of inlet pressure, P_L, viscosity of adhesive, μ, n, and the radius of needle, R_n.

4.1.2. Model Simulation

The commercial FEA code Adina was adopted to accomplish the simulation of all three flow models. In this pipe flow model, we only computed the fluid domain of the middle transition section and bottom needle section according to Section 4.1.1. The enclosed area was represented by P_L at the upper inlet and P_0 at the bottom outlet.

The velocity field of the pipe flow is shown in a vector plot in Fig. 8. The flow velocity in the needle along the z-direction described by

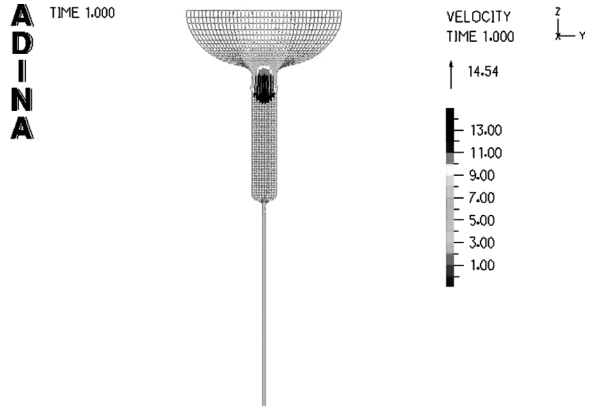

FIGURE 8 Velocity field of pipe flow.

Eq. (10) has a distribution in the form of a parabola in the r-direction, as shown in Figure 9; the simulation data are shown by small stars connected with a polygonal line. It is easily found that the two results are quite close, which indicates that the volumetric flow rate Eq. (11) obtained from the velocity, u_z, is quite precise and can be used in the analysis of the next sub-process.

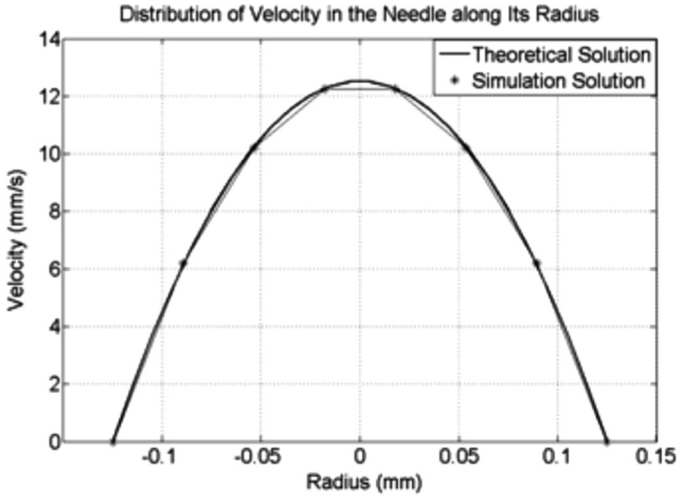

FIGURE 9 Comparison of theoretical and simulation solutions for flow velocity.

4.2. Planar Spreading

4.2.1. Modelling of Planar Spreading

In accordance with the spreading characteristics of the adhesive, the following assumptions were made:

i. The process of spreading of the adhesive is isothermal.
ii. The boundary effect in a line of adhesive can be ignored, and only the spreading of the main part of a line of adhesive needs to be considered.
iii. For each long adhesive line, since the horizontal dimension is far greater than the vertical one, we only need to consider the vertical spreading, which is perpendicular to the horizontal direction of the adhesive line.
iv. Each adhesive line spreads symmetrically from its central axis.

Owing to the similarity of all bonding operations in this study, we analysed only one example (Fig. 10). Here, two long lines of adhesive spread towards each other and finally meet each other at the line of contact. The core task was to investigate the spreading process of the adhesive line at a particular cross-section. We took half a cross-section as the model, as shown in Figure 11. Analysing this is the key problem for this spreading process. It is the motion of a non-Newtonian fluid, which is unsteady and has a moving boundary in the form of a free surface.

4.2.2. Numerical Solution

The FEA code Adina was adopted to trace the moving interface between the adhesive and the air; the code is based on the method of volume of fluid (VOF) [54]. Gravity and atmospheric pressure were included in the model, and the surface tension of the adhesive was applied at the interface. The initial shape of the half cross-section was set to be an arc in the form of a quarter ellipse; the semi-major axis, a, and the semi-minor axis, b, were obtained from the following

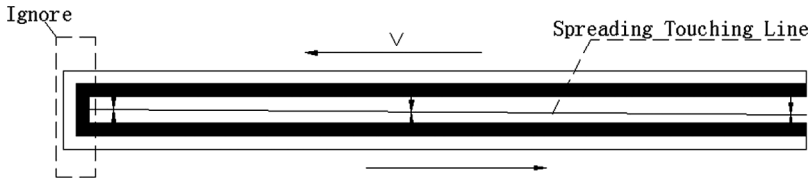

FIGURE 10 Illustration of spreading of two lines of adhesive.

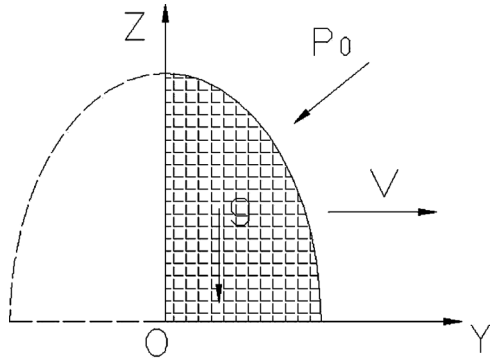

FIGURE 11 Diagram of spreading in half a cross-section.

equation:

$$\frac{Q}{V_n} = \frac{\pi \cdot ab}{2}, \tag{12}$$

where Q is the volumetric flow rate and V_n is the speed of motion of the needle. According to the above given values of all relevant parameters, we could obtain that a was 0.35 mm, and b was 0.22 mm.

The spreading process is shown in Figure 12, in which the bottom left area enclosed by a black line shows the initial shape of the fluid flow and the white area shows the status of the flow of the adhesive.

4.2.3. Validation by Experiments

A CCD camera was employed to record the micro movement of planar spreading of the adhesive and through image processing we

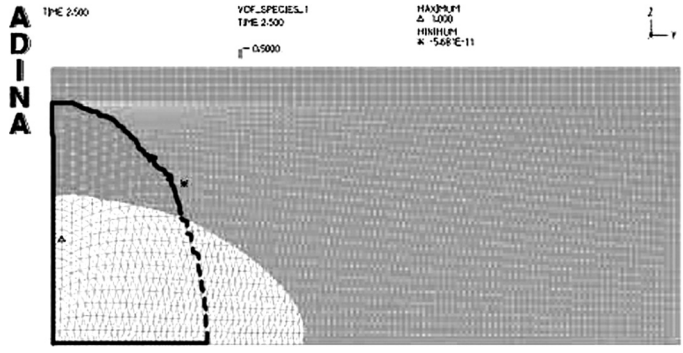

FIGURE 12 Planar spreading of adhesive.

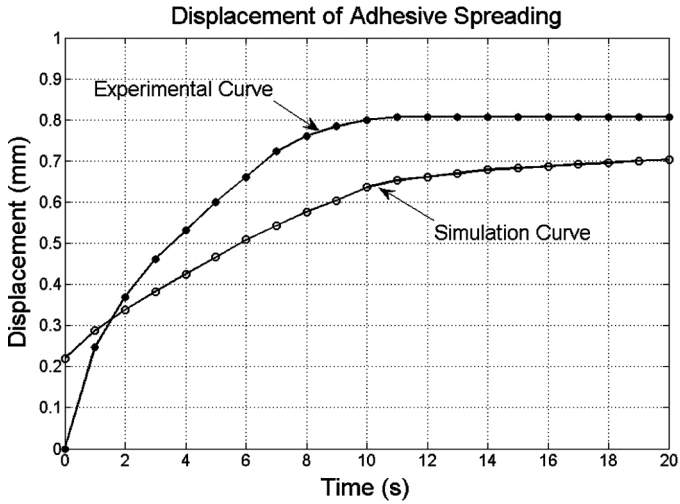

FIGURE 13 Displacement of spreading of adhesive.

extracted the displacement of the moving boundary of the standard spreading model changing with time (Fig. 13). The simulation data were obtained from the post-processing module of Adina. It may be seen that the velocity of the spreading of the adhesive gradually diminishes, and approaches zero at about the 12th second. Thus, the moving boundary stops at a position 0.7–0.8 mm away from the axis, which demonstrates the effect of the surface tension of the adhesive. Comparing the two curves in Figure 13, we may draw the conclusion that the results of the simulation and experiment are quite close, and that the correctness of the simulation is basically validated by the experiment. The difference between them comes mainly from measurement error and the numerical computational method.

4.2.4. Prediction of the Shape of the Adhesive Layer

The back-and-forth pattern of application of the adhesive deposited on the solar cell is shown in Figure 3b, of which there are three parameters to be adjusted: the number of lines of adhesive, n_c, the spacing between lines, D, and the distance from the edge, δ. Since the time of spreading of the adhesive, t_s, was set to 4 minutes, the adhesive lines spread so as to mix together to become a uniform layer before the bonding operation. According to our standard spreading model, the boundary of the adhesive layer moved only for 12 seconds and then stopped. Thus, we obtained the position of the boundary of the

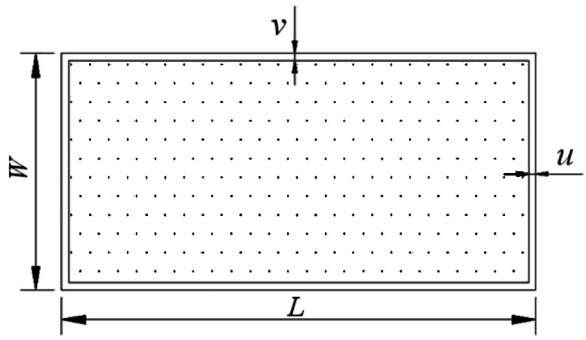

FIGURE 14 Outline of the adhesive layer.

adhesive layer by means of two different initial spacings δ (δ_1, δ_2) minus the adhesive's maximum spreading displacement, 0.8 mm Figure 14, and the two spacings at the margin in the figure are $u = 0.6$ mm and $v = 0.65$ mm.

4.3. Automated Bonding

The bonding operation is the most important one in the whole adhesion process, as it depends upon the spreading borders, thickness and uniformity of the adhesive layer, the edge-alignment between the cover glass and the solar cell, and air bubbles in the adhesive layer. Dealing with the problem of air bubbles is a very important task and will be studied in more detail in future work. The present article analyzes only the adhesive layer's spreading boundaries, its thickness and uniformity, and the edge-alignment between the cover glass and the solar cell.

4.3.1. Constitutive Relationship for the Four Parts

4.3.1.1. Vacuum Suction Cup. The vacuum suction cup is made of nitrile butadiene rubber (NBR); the shape at the end of it is like a bowl (see Fig. 15). Researchers usually investigate the nonlinear elastic behavior of rubber materials under static loads. As an isotropic, super-elastic material [55], the constitutive relation for rubber is generally represented by the function of strain energy density. Two widely used models in engineering are the Ogden and Mooney-Rivlin models [55–56]. However, these models are relatively complicated, and their material constants generally do not have obvious physical meanings [56–57]. In addition, it is difficult to conduct experiments to obtain those material parameters.

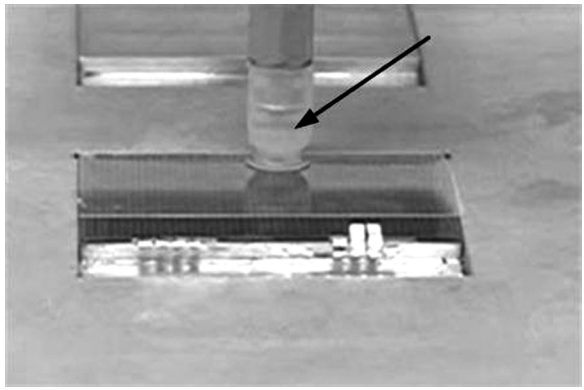

FIGURE 15 Vacuum suction cup in the bonding operation.

We adopted an isotropic, nonlinear elastic model to simulate the constitutive behaviour of the suction cup. By using experiments on the relation of a suddenly increased deformation of the suction cup to a non-zero initial strain and the consequent elastic force (Fig. 16), we obtained a function of deformation, ΔX, and elastic force, F, at a negative gas pressure of $-42\,\text{kPa}$, as shown in Eq. (13), and accordingly derived a nonlinear constitutive relation for the vacuum suction cup at the negative gas pressure of $-42\,\text{kPa}$, as shown in Eq. (14). σ represented the stress of the vacuum suction cup due to deformation, and ε expressed the strain of the suction cup accordingly. The density, ρ, of the vacuum suction cup was $1.2 \times 10^3\,\text{kg/m}^3$.

$$F = \begin{cases} 0, & 0 \le \Delta X \le 0.0258 \\ 1.0609 \cdot \Delta X^2 + 1.3458 \cdot \Delta X - 0.0355, & 0.0258 < \Delta X < 1.00 \\ 2.3712, & 1.00 \le \Delta X \le 1.44 \end{cases} \quad (13)$$

$$\sigma = \begin{cases} 0 & 0 \le \varepsilon \le 0.0022 \\ 5293500 \cdot \varepsilon^2 + 559580 \cdot \varepsilon - 1230, & 0.0022 < \varepsilon < 0.084 \\ 83126, & 0.084 \le \varepsilon \end{cases} \quad (14)$$

4.3.1.2. Anti-Irradiation Cover Glass. The anti-irradiation cover glass was thin, 0.1–0.15 mm in thickness, and was of several different types. It could be regarded as an isotropic, linear elastic material, whose elastic modulus, E, was $4.15 \times 10^9\,\text{Pa}$, Poisson's ratio, λ, was 0.33, and density, ρ, was $2.53 \times 10^3\,\text{kg/m}^3$.

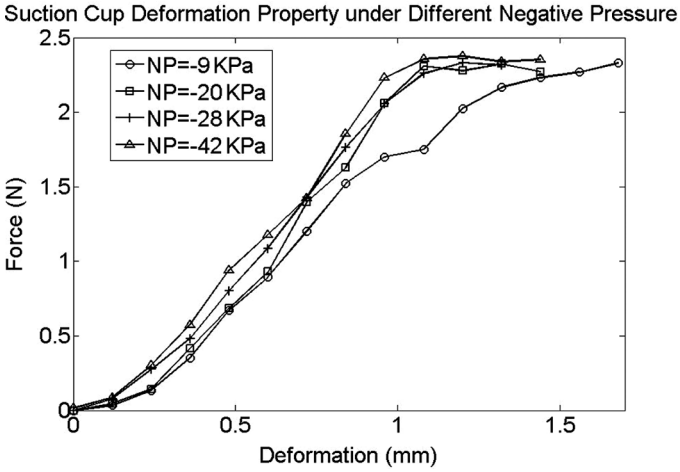

FIGURE 16 Relation of new increased deformation and elastic force under different negative gas pressure.

4.3.1.3. Silicone Adhesive. The silicone adhesive deposited onto the solar cell to bond a cover glass to it could be represented as a linear viscoelastic material *e.g.*, a Maxwell fluid [58], with the constitutive equation used in computation expressed as follows [59]:

$$\begin{aligned} \tau_{ij}(t) &= 2G(0)\cdot e_{ij}(t) + 2\int_{0^+}^{t} e_{ij}(t-\tau)\frac{dG(\tau)}{d\tau}d\tau, \\ \sigma_{kk}(t) &= 3K(0)\cdot e_{kk}(t) + 3\int_{0^+}^{t} \varepsilon_{kk}(t-\tau)\frac{dK(\tau)}{d\tau}d\tau \quad i,j,k = 1,2,3, \end{aligned} \tag{15}$$

where t is the time, τ_{ij} is the deviatoric stress, σ_{kk} is the normal stress, e_{ij} is the deviatoric strain, e_{kk} is the diagonal element of e_{ij}, ε_{kk} is the normal strain, $G(t)$ is the shear modulus, and $K(t)$ is the bulk modulus. Two important constitutive parameters are the shear modulus, $G(t)$, and the bulk modulus, $K(t)$. The reader can refer to the experimental investigations of the silicone adhesive described in Section 2.3.

4.3.1.4. Space Solar Cell. The solar cell was held solidly by suction to the orientation plate. Therefore, the solar cell could be considered as a rigid body, without any deformation or movement.

4.3.2. Systematic Model of the Bonding Process

A dynamic model of the physical bonding process was created, as shown in Figure 17. The input was the displacement of the suction cup in the

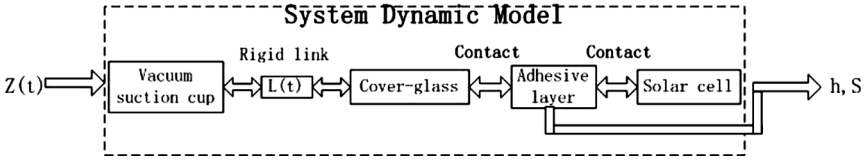

FIGURE 17 Dynamic model of the bonding process.

z-direction, controlled by the robot (the covering speed was V_b, and t_b and t_w were the covering time and suspending time, respectively), and the outputs were the thickness, h, the uniformity, the spreading boundary, S, of the adhesive layer and the edge-alignment of the cover glass with the solar cell. In the model, there were four parts and the relations between each of them. There was a rigid link, $L(t)$, between the suction cup and the cover glass, which would be cancelled at some time, t_1, controlled by the robot. The most impressive characteristic of the model was the strong contact effect, between the cover glass and the adhesive layer and between the adhesive layer and the solar cell. A group of values of operating parameters were given: $V_b = 0.1\,\text{mm/s}$, $t_b = 6\text{s}$, $t_w = 2\text{s}$, $t_1 = 8s, L(t) = \begin{cases} 1, t \le t_1 \\ 0, t > t_1 \end{cases}, \alpha = 10^\circ$.

4.3.3. Numerical Simulation and Experimental Validation

The purpose of numerical simulation was to acquire information on the thickness, h, the uniformity, the spreading boundary, S, of the adhesive layer, and the edge-alignment of the cover glass with the

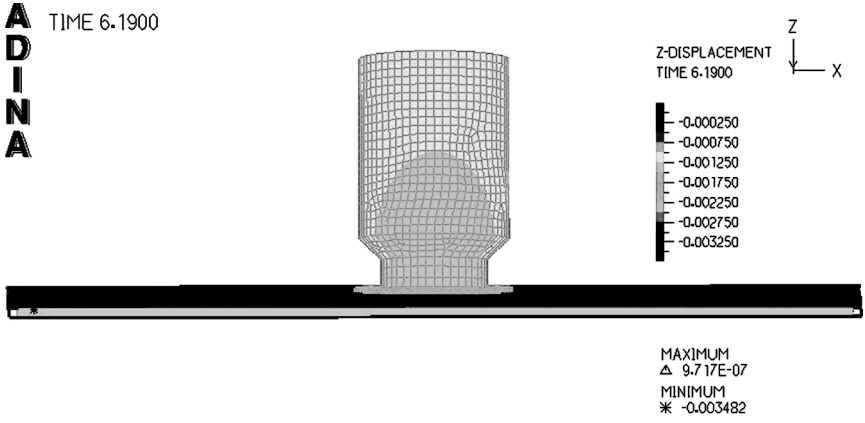

FIGURE 18 Finite element analysis of the bonding process.

TABLE 4 Simulation Thickness of the Adhesive Layer

Position	Thickness (μm)
Top left corner	113
Top right corner	112
Centre	112
Bottom left corner	116
Bottom right corner	116

solar cell. In the established FEA model, two pairs of contact surfaces were defined: the contact between the cover glass and the adhesive layer, and the contact between the adhesive layer and the solar cell. All the faces of the adhesive layer were assigned a surface tension. The initial shape of the adhesive layer was discussed in Section 4.2.4 (Fig. 14). A simulation image of the bonding operation was shown in Figure 18.

The results of the simulation were as follows. The cover glass was aligned with the solar cell below by means of interaction with the middle adhesive layer; this was called a 'self-alignment' phenomenon, and its mechanism needed to be further investigated. All the adhesive filled the clearance between the cover glass and the solar cell, except for a very small amount of overflow in some places, which sometimes happened in real operations. For the thickness and uniformity of the adhesive layer in the simulation model, we took samples at five positions in the adhesive layer, and the corresponding thicknesses are shown in Table 4. It can be seen that the thicknesses are close, except that the values in places at the top were a little smaller than those in places at the bottom. Experimental results showed that the thickness of the adhesive layer was uniform, and the average value was 112 μm. Obviously, the simulation results were close to the experiments.

5. CONCLUSIONS

Through an analysis and comparison of several adhesive coating and bonding techniques, we have developed a process to bond anti-irradiation cover glasses to space solar cells. An automated coating and bonding system has implemented this process to manufacture bonded solar cells. Compared with a manual method of implementing the process, the automated system produced excellent performance in terms of meeting the requirements for the finished products. Also, we have created models of the flow of the silicone adhesive for the three

TABLE 5 Bonding Quality Function Q_b and Parameters

Q_b	Paramenters (pipe flow)	Paramenters (planar spreading)	Paramenters (automated bonding)
Thickness	P_L	V_n	α
Uniformity	$\eta(\mu, n)$	D	V_b
Area	R_n	δ	t_b
Edge-alignment		n_c	t_w
...		t_s	

sub-processes of the process, and performed analysis and validation *via* the three aspects of theory, simulation, and experiment. We have developed a function, Q_b, that describes the quality of the adhesive bond in the form of Q_b(thickness, uniformity, area, edge-alignment) = $f(P_L, \eta(\mu, n), R_n, V_n, D, \delta, n_c, t_s, \alpha, V_b, t_b, t_w)$ (Table 5). Performing a parametric study and identifying the contribution of each parameter to Q_b is our next research focus. Meanwhile, a simulation platform for the whole adhesion process has been created, to allow us to evaluate and predict the adhesion quality of solar cells when the dimensions of the cells and the adhesive are changed. Future directions for research include the problem of air bubbles in the bonding process, the evaluation and prediction of the adhesion quality of bonded solar cells of different dimensions, and the optimization of the parameters of the whole adhesion process.

ACKNOWLEDGMENTS

This work was partially supported by the National Natural Science Foundation of China under Grant No. 60675040. The authors are thankful to the Shanghai Institute of Space Power in Shanghai, China, for providing the experimental support.

REFERENCES

[1] Hayaawa, T., Nasuno, Y., Kondo, M., and Matsuda, A., *J. Shapu Giho/Sharp Tech.* **83**, 45–48 (2002).
[2] Wojtczuk, S. and Reinhardt, K., *Proc. 25th IEEE Photovoltaic Specialists Conf. Rec.*, (Washington D.C, 1996). pp. 49–52.
[3] Iles, P. A., *Solar Energy Materials & Solar Cells* **68**, 1–13 (2001).
[4] Li, G. X., *Aerospace Shanghai* **3**, 42–48 (2002).
[5] Wang, R. and Si, G. L., *J. Beijing Norm Univ. (Natural Sci.)* **37**(4), 507–510 (2001).
[6] Yang, Q. H., Master's thesis, Shanghai Jiao Tong University, Shanghai, China (2004).

[7] White, P. A. and Jones, D. E., *22nd IEEE Photovoltaic Specialists Conf. Rec.*, (Las Vegas, NV, 1991), pp. 1508–1511.
[8] Mullaney, K., Dollery, A. A., Jones, G. M., and Bogus, K., *23rd IEEE Photovoltaic Specialists Conf. Rec.*, (Louisville, KY, 1993). pp. 1392–1398.
[9] Kitchen, C. A., Dollery, A. A., and Bogus, K., *24th IEEE Photovoltaic Energy Conversion Conf. Rec.,* (Waikoloa, HI, 1994), pp. 2058–2061.
[10] White, P. A., *21st IEEE Photovoltaic Specialists Conf. Rec.*, (Kissimmee, FL, 1990), pp. 1300–1303.
[11] Nowlan, M. J., Tobin, S. P., and Darkazalli, G., *22nd IEEE Photovoltaic Specialists Conf. Rec.*, (Las Vegas, NV, 1991), pp. 1480–1484.
[12] Koch, J. W. and White, P. A., *21st IEEE Photovoltaic Specialists Conf. Rec.*, (Kissimmee, FL, 1990), pp. 1294–1299.
[13] Hardingham, C., Hayward, A., Cross, T. A., and Goodbody, C., *24th IEEE Photovoltaic Energy Conversion Conf. Rec.*, (Waikoloa, HI, 1994), pp. 2217–2219.
[14] Xiong, X. Y., *World of Printing* **3**, 20–21 (2001).
[15] Huang, Y. Y. and Chou, K. S., *Ceramics Inter.* **29**, 485–493 (2003).
[16] Tsai, S. W. and Chang, T. A., *J. Chromatography A* **954**, 191–198 (2002).
[17] Frank, M., Lachenmeier, D. W., Kroener, L., and Madea, B., *J. Chromatography A* **958**, 231–238 (2002).
[18] Giovanni, V., Christopher, F., Ahluwalia, A., and Sangeeta, B., *Biomaterials* **24**, 2533–2540 (2003).
[19] Fu, Z., Zhao, Y. Z., Yang, Q. H., Cao, Q. X., Chen, M. B., Zhang, J., and Tang, Z. Q., *Robotica* **23**, 561–565 (2005).
[20] Zhao, Y. Z., Fu, Z., Cao, Q. X., Chen, M. B., Zhang, J., and Tang, Z. Q., *J. Shanghai Jiao Tong Univ.* **39**(6), 888–891 (2005).
[21] Fu, Z., Zhao, Y. Z., and Yang, Q. H., *J. Manufacturing Sci. and Engi. ASME* **128**(2), 576–579 (2006).
[22] Dhere, G. N. and Raravikar, R. N., *Solar Energy Materials & Solar Cells* **67**(4), 363–367 (2001).
[23] Dhere, G. N., Wollam, E. M., and Gadre, S. K., *Proc. IEEE 26th Photovoltaic Specialists Conf. Rec.*, (Anaheim, CA, USA, 1997), pp. 1217–1220.
[24] Laxmi, S., Nitin, K., Nilesh, K., Pinto, R., Dusane, R. O., and Schroder, B., *Thin Solid Films* **501**(2), 117–120 (2006).
[25] Zhang, L. X., Yang, S. Q., and He, S. Y., *ACTA Energiae Solaris Sinica* **23**(3), 297–300 (2002).
[26] Blake, I. N., III, *Proc. 32nd Intersociety Energy Conversion Engineering Conf.*, (Honolulu, HI, USA, 1997), pp. 395–400.
[27] Scheiman, D. A., Smith, B. K., Kurland, R. M., and Mesch, H. G., *Proc. 25th Intersociety Energy Conversion Engineering Conf.*, (Reno, NV, USA, 1990), pp. 575–580.
[28] Akter, S. and Hashmi, M. S., *J. Progress in Organic Coating* **37**, 15–22 (1999).
[29] Greener, J. and Middleman, S., *Industrial and Engi. Chemistry Fund* **20**(1), 63–66 (1981).
[30] KuZilati, K., Pandey, P., Song, Y. X., and Richard, T., *Powder Tech.* **166**, 81–90 (2006).
[31] Ronsse, F., Pieters, J. G., and Dewettinck, K., *J. Food Engi.* **78**, 296–307 (2007).
[32] Ronsse, F., Pieters, J. G., and Dewettinck, K., *J. Food Engi.* **78**, 308–322 (2007).
[33] Shah, U., Zhu, J., Zhang, C., and Nother, J. H., Sr., *Powder Tech.* **164**, 22–32 (2006).
[34] Beeley, N. R. F. and Guo, Z. X., *Materials Sci. and Engi.* **365**, 341–348 (2004).
[35] Fourcade, E., Bertrand, F., Reglat, O., and Tanguy, P. A., *Comp. Methods in Appl. Mech. Engi.* **174**, 235–245 (1999).

[36] Hewson, R. W., Kapur, N., and Gaskell, P. H., *Chemical Engi. Sci.* **61**, 5487–5499 (2006).
[37] Grayeli, N., Ellis, L., and Jasper, J., *IEEE/CHMT '91 IEMT Symposium*, (New York, NY, 1991), pp. 15–20.
[38] Huang, Y. Y. and Chou, K. S., *Ceramics Inter.* **29**, 485–493 (2003).
[39] Timmons, M. L., *Proc. IEEE Aerospace Conf.*, (Snowmass at Aspen, CO, 1998), pp. 131–140.
[40] Freundlich, A., Newman, F., Vilela, M. F., Monier, C., Aguilar, L., and Street, S., *J. Crystal Growth* **209**, 481–485 (2000).
[41] Taira, S., Tsukiji, M., and Matsui, T., *Tech. Digest of the Inter PVSEC-II*, (Hokkaido, Sapporo, Japan, 1999), p. 189.
[42] Yanmanoto, K., Yoshimi, M., and Suzuki, *2nd Word Conf and Exhibition on Photovoltaic Solar Energy Conversion*, (Vienna, Austria, 1998), p. 1284.
[43] Kaneiwa, M. and Kamimura, K., *J. Shapu Giho/Sharp Tech.* **83**, 54–57 (2002).
[44] Wang, Y. D., Cui, R. Q., and Xu, X. Q., *Power Supply Tech.* **25**, 182–184 (2001).
[45] Liang, Z. C. and Xu, Y., *Transaction of Solar Energy* **23**(1), 45–47 (2002).
[46] Green, Martin A., *Proc. 2003 Anniversary Solar Energy Conf of China Solar Energy Society*, (Shanghai, P.R. China, 2003), pp. 2–8.
[47] Hardingham, C., Huggins, C. R., Simpson, J. W., and Cross, T. A., *25th IEEE Photovoltaic Specialists Conf. Rec.*, (Washington, DC, 1996), pp. 255–258.
[48] Hidetaka, T. and Ryuichi, S., *IEEE Electron Device Letters* **21**(8), 387–389 (2000).
[49] Catalano, A., *24th IEEE Photovoltaic Energy Conversion Conf. Rec.*, (Waikoloa, HI, 1994), pp. 52–59.
[50] Lt, J. and Tringe, W., *Proc. IEEE Aerospace Conf.*, (Big Sky, MT, 2000), pp. 61–68.
[51] Zhang, L. X., Yang, S. Q., He, S. Y., and Yang, D. Z., *Rubber Industry* **49**, 503–507 (2002).
[52] Han, S. F., *Constitutive Eq of Non-Newtonian Fluid and Theory of Symbolic Comp* (Press of Science, Beijing, 2000).
[53] Ostwald, W. and de Waele, A., *J. Chem. Assoc.* **6**, 23 (1923).
[54] Liu, R. X. and Wang, Z. F., *Numerical Simulation Method and Moving Interface Tracing* (Press of Chinese Univ. of Sci. and Tech., Hefei, 2001).
[55] Li, X. F. and Yang, X. X., *China Elastomerics* **15**(1), 50–58 (2005).
[56] Mackerle, J., *Modelling Simul. Mater. Sci. Eng.* **12**, 1031–1053 (2004).
[57] Zhao, J. C. and Zhou, C. X., *China Elastomerics* **14**(6), 26–30 (2004).
[58] Zhou, G. Q. and Liu, X. M., *Viscoelastic Theory* (Press of Chinese Univ. of Sci. and Tech., Hefei, 1996).
[59] Findley, W. N., Lai, J. S., and Onaram, K., *Creep and Relaxation of Nonlinear Viscoelastic Materials*, (Dover Publications, Mineola, 1976).